Inorganic Chemistry

ARTICLE

pubs.acs.org/IC

Dipeptide-Based Models of Nickel Superoxide Dismutase: Solvent Effects Highlight a Critical Role to Ni−S Bonding and Active Site Stabilization

Eric M. Gale, Darin M. Cowart, Robert A. Scott, and Todd C. Harrop*

Department of Chemistry, The University of Georgia, 1001 Cedar Street, Athens, Georgia 30602, United States

Supporting Information

ABSTRACT: Nickel superoxide dismutase (Ni−SOD) catalyzes the disproportionation of the superoxide radical to O_2 and H_2O_2 utilizing the Ni(III/II) redox couple. The Ni center in Ni−SOD resides in an unusual coordination environment that is distinct from other SODs. In the reduced state (Ni−SOD_{red}), Ni(II) is ligated to a primary amine-N from His1, anionic carboxamido-N/thiolato-S from Cys2, and a second thiolato-S from Cys6 to complete a NiN_2S_2 square-planar coordination motif. Utilizing the dipeptide N_2S^{2-} ligand, H_2N-Gly-L-Cys-OMe (GC-$OMeH_2$), an accurate model of the structural and electronic contributions provided by His1 and Cys2 in Ni−SOD_{red}, we constructed the dinuclear sulfur-bridged metallosynthon, $[Ni_2(GC\text{-}OMe)_2]$ (**1**). From **1** we prepared the following monomeric Ni(II)−N_2S_2 complexes: K[Ni(GC-OMe)(SC_6H_4-*p*-Cl)] (**2**), K[Ni(GC-OMe)(S^tBu)] (**3**), K[Ni(GC-OMe)(SC_6H_4-*p*-OMe)] (**4**), and K[Ni(GC-OMe)(SNAc)] (**5**). The design strategy in utilizing GC-OMe^{2-} is analogous to one which we reported before (see *Inorg. Chem.* **2009**, *48*, 5620 and *Inorg. Chem.* **2010**, *49*, 7080) where Ni−SOD_{red} active site mimics can be assembled at will with electronically variant RS^- ligands. Discussed herein is our initial account pertaining to the aqueous behavior of isolable, small-molecule Ni−SOD model complexes (non-maquette based). Spectroscopic (FTIR, UV−vis, ESI-MS, XAS) and electrochemical (CV) measurements suggest that **2**−**5** successfully simulate many of the electronic features of Ni−SOD_{red}. Furthermore, the aqueous studies reveal a dynamic behavior with regard to RS^- lability and bridging interactions, suggesting a stabilizing role brought about by the protein architecture.

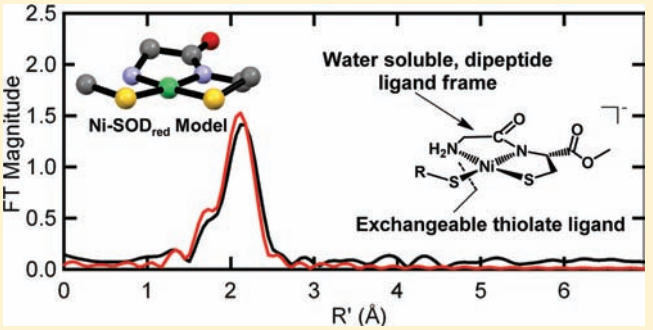

INTRODUCTION

The cytotoxic superoxide anion radical ($O_2^{\bullet-}$) is an inevitable byproduct of aerobic metabolism that is capable of effecting significant cellular damage if not tightly regulated.[1−3] In fact, increased production of superoxide has been associated with carcinogenesis,[4,5] post-ischemic tissue damage,[3,6] and neurodegenerative diseases such as Parkinson's[7,8] and Alzheimer's.[3,9] To maintain safe concentrations of intracellular $O_2^{\bullet-}$ ($\sim 10^{-10}$ M), aerobic organisms employ superoxide dismutases (SODs), enzymes that catalyze the diffusion-controlled (10^9 M^{-1} s^{-1}) disproportionation of $O_2^{\bullet-}$ to O_2 and H_2O_2.[10] All SODs possess a transition metal in their active site, which catalyzes the disproportionation reaction by toggling between oxidized and reduced states as demonstrated in Scheme 1. Over the years, a rich knowledge of SODs employing redox-active Fe,[11,12] Mn,[13] and Cu[14] has accumulated. However, less is understood about the newly discovered Ni−SOD, which is isolated from certain *Streptomyces* microbial strains[15,16] and also believed to be utilized by cyanobacteria.[17]

The Ni−SOD enzyme is strikingly different from other known SODs. Crystallographic characterization reveals the Ni ion within a nine residue (HCDLPCGVY) "Ni-hook motif". In its reduced Ni(II) state, the metal is bound by the N-terminal amine of His1, the anionic carboxamido-N from Cys2, and the cysteine thiolates of Cys2 and Cys6 to complete an N_2S_2 square-planar geometry (Chart 1).[18,19] In its oxidized Ni(III) state, the coordination geometry is square pyramidal with the imidazole-N of His1 occupying the apical position (Chart 1).[18,19] Although a growing body of protein,[15,16,20−26] polypeptide maquette,[27−34] and small-molecule[35−41] literature has shed some light upon the role of this unusual donor set, many outstanding questions remain as to the interplay between the Ni ion, ligands, secondary coordination sphere, substrate, and products during SOD catalysis.[20−30,35−39,42−44]

While several redox-active Ni-containing enzymes are known,[45−49] coordination of cysteine thiolates appears to be a reoccurring

Scheme 1. Chemistry Catalyzed by SOD Split into Half Reactions

$$M^{ox} + O_2^{\bullet-} \longrightarrow M^{red} + O_2 \quad (1)$$

$$M^{red} + O_2^{\bullet-} + 2\,H^+ \longrightarrow M^{ox} + H_2O_2 \quad (2)$$

Received: July 29, 2011
Published: September 20, 2011

dx.doi.org/10.1021/ic2016462 | *Inorg. Chem.* 2011, 50, 10460–10471

Chart 1. (Top) Active Site of Ni−SOD$_{ox}$ (left), Ni−SOD$_{red}$ (middle), and Ni−SOD$_{red}$ Analogues Described in the Present Work, [Ni(GC-OMe)(SR)]$^-$ (right). (Bottom) R groups used in this study

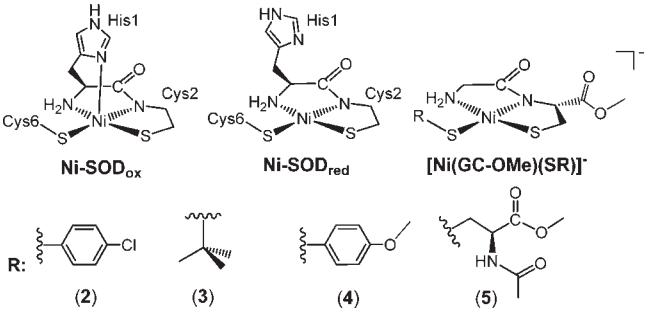

feature, presumably in order to depress the redox couples required to achieve both high Ni(III) and low Ni(I) oxidation states toward physiologically accessible potentials.[50,51] Intriguingly, the majority of these enzymes catalyze reactions of great environmental and economical importance, such as the equilibration of CO_2 and CO for utilization as one-carbon equivalents[47] and consumption and generation of H^+ and H_2.[45] In NiFe−hydrogenase and Ni−SOD, the thiolate ligands have been implicated as active players in the catalytic cycle performing roles beyond redox modulation, including H^+ storage and transport.[26,52−54] The unusual coordination observed at the Ni−SOD active site has provided a novel platform for synthetic chemists to model and gain a basic understanding of such interactions. The fundamental role of the atypical donor set, in conjunction with the obvious relevance of SOD to health and medicine,[4−9] has provided motivation for modeling studies pertaining to this unique metalloenzyme.

Previously, we reported a general and facile route toward Ni−SOD$_{red}$ model complexes utilizing the tridentate N_2S ligand nmp^{2-} (where nmp^{2-} is the dianion of *N*-(2-mercaptoethyl)picolinamide) that models the basal plane contributions of His1 and Cys2.[38,39] The exogenously added monodentate thiolate ligand in these [Ni(nmp)(SR)]$^-$ complexes (where RS$^-$ models Cys6) can be systematically substituted via a variety of synthetic protocols. This feature was exploited to obtain a library of [Ni(nmp)(SR)]$^-$ complexes with electronically variant monodentate thiolates, which incorporate second-sphere functionalities tethered via the exogenously added thiolate. This study was fruitful in that it allowed for an in-depth analysis as to the effects manifested by intramolecular hydrogen bonding/thiolate protonation on the structural, spectroscopic, and reactivity properties of NiN_2S_2 complexes related to Ni−SOD$_{red}$. For example, we demonstrated that H-bonding to Ni-coordinated thiolates promotes more metal-based reactivity via reduction of S-contributions to the HOMO (relative to Ni) as well as by decreasing the electrostatic potentials of the coordinated thiolates.[38] Unfortunately, the [Ni(nmp)] series of complexes suffer from poor solubility and stability in aqueous solution, thus limiting reactivity studies to organic solvents.

The objective of the present work was to prepare small-molecule [Ni(N_2S)(SR)]$^-$ complexes of variant RS$^-$ (similar to the Ni(nmp) system) as Ni−SOD models that could be studied in a biologically relevant aqueous environment. To this end, we utilized the dipeptide N_2S ligand, H_2N-Gly-L-Cys-OMe (abbreviated as GC-OMeH_2, where H represents dissociable protons), as a suitable water soluble construct to prepare the dinuclear metallosynthon, [Ni_2(GC-OMe)$_2$] (**1**). Complex **1** was then used as a direct precursor toward the Ni−SOD model complexes, K[Ni(GC-OMe)(SC_6H_4-*p*-Cl)] (**2**), K[Ni(GC-OMe)(S^tBu)] (**3**), K[Ni(GC-OMe)(SC_6H_4-*p*-OMe)] (**4**), and K[Ni(GC-OMe)(SNAc)] (**5**) (Chart 1). These monomeric Ni(II) complexes were prepared via methodologies previously described by us.[38,39] The present study is among the few regarding the characterization of discrete isolable Ni−SOD analogues in an aqueous environment (low MW containing only one peptide linkage; non-maquette based) providing for the use of small-molecule characterization techniques in aqueous media, which has been utilized exclusively for tripeptide[33,34] and polypeptide maquette Ni−SOD analogues.[27−30] The synthesis, structure, and properties of **1**−**5** are discussed in this work. The results obtained shed light on the behavior of species electronically analogous to the Ni−SOD$_{red}$ active site under pseudo-physiological conditions when stripped of their macromolecular surroundings.

EXPERIMENTAL SECTION

General Information. All reagents were purchased from commercial suppliers and used as received unless otherwise noted. Acetonitrile (MeCN), methylene chloride (CH_2Cl_2), tetrahydrofuran (THF), diethyl ether (Et_2O), and pentane were purified by passage through activated alumina columns using an MBraun MB-SPS solvent purification system and stored under a dinitrogen (N_2) atmosphere before use. *N*,*N*′-dimethylformamide (DMF) was purified with a VAC Solvent Purifier containing 4 Å molecular sieves and stored under similar conditions. Triethylamine (TEA) was dried over Na_2SO_3. Anhydrous MeOH was obtained by distilling from Mg(OMe)$_2$ under an N_2 atmosphere. All reactions were performed under an inert atmosphere of N_2 using standard Schlenk line techniques or in an MBraun Unilab glovebox under an atmosphere of purified N_2. Potassium salts of the monodentate thiolate ligands were prepared according to a modified literature procedure[55] via addition of 1 mol-equiv of K(0) to the appropriate thiol in dry MeOH.

Physical Methods. FTIR spectra were collected on a Thermo-Nicolet 6700 spectrophotometer running the OMNIC software; samples were prepared as pressed KBr pellets. Electronic absorption spectra were run at 298 K using a Cary-50 spectrophotometer containing a Quantum Northwest TC 125 temperature control unit. The UV−vis samples were prepared in gastight Teflon-lined screw cap quartz cells with an optical pathlength of 1 cm equipped with a rubber septum. Cyclic voltammetry (CV) measurements were performed with a PAR model 273A potentiostat using a Ag/Ag$^+$ (0.01 M $AgNO_3$/0.1 M ^{n}Bu$_4$NPF$_6$ in MeCN) reference electrode, Pt counter electrode, and glassy carbon millielectrode (2 mm) as the working electrode when measuring in DMF. An Ag/AgCl reference electrode was used when measuring the aqueous samples. Measurements were performed at ambient temperature using 5.0 mM analyte in the appropriate Ar-purged solvent containing 0.1 M ^{n}Bu$_4$NPF$_6$ as the supporting electrolyte in DMF or 0.5 M KNO_3 for aqueous measurements. The "Maximize Stability" mode was utilized in the PAR PowerCV software utilizing a low-pass 5.3 Hz filter. To ensure accuracy in the measured CVs, these experiments were performed in triplicate while polishing the working electrode between each run, and we report an average E_{ox}. Additionally, potentials were checked and corrected by recording the CV of a ferrocene standard in DMF or a potassium ferricyanide standard in aqueous conditions (referenced to the ferro/ferricyanide couple in 50 mM pH 7.0 phosphate buffer)[56] under the same conditions as the complexes before each run. NMR spectra were recorded in the listed deuterated solvent on a 400 MHz Bruker BZH 400/52 NMR

dx.doi.org/10.1021/ic2016462 |*Inorg. Chem.* 2011, 50, 10460–10471

spectrometer or 500 MHz Varian Unity INOVA NMR spectrometer at ambient temperature with chemical shifts referenced to TMS or residual protio signal of the deuterated solvent. Low-resolution ESI-MS data were collected using a Perkin-Elmer Sciex API I Plus quadrupole mass spectrometer and high-resolution ESI-MS data were collected using a Bruker Daltonics 9.4 T APEX Qh FT-ICR-MS. Elemental analysis for C, H, and N was performed at QTI-Intertek in Whitehouse, NJ.

Synthesis of H_2N-Gly-L-Cys-OMe·TFA (GC-OMe·TFA). Synthesis of the ligand comprised the following steps.

Step 1. H_2N-L-Cys(STrit)-OMe. To a batch of 13.701 g (52.629 mmol) of triphenyl methanol dissolved in 50 mL of trifluoroacetic acid (TFA) was added 9.095 g (52.99 mmol) of L-cysteine methyl ester hydrochloride forming a red-orange solution. The resultant solution was left to stir at room temperature for 1 h before it was concentrated to an orange oil, which was partitioned between 300 mL of CH_2Cl_2 and 300 mL of H_2O, resulting in bleaching of the orange color. Portions of K_2CO_3 were then slowly added to the aqueous layer until a basic pH was sustained for up to 1 h. The organic layer was then separated, washed with saturated $NaHCO_3$(aq) and brine, dried over $MgSO_4$, and concentrated to a pale oil which solidified after overnight stirring in hexanes. The white solids thus obtained were isolated via vacuum filtration (16.104 g, 42.660 mmol, 81%). Mp: 57−58 °C. ^{1}H NMR (400 MHz, $CDCl_3$, δ from TMS): 7.48 (d, 6H), 7.32 (t, 6H), 7.25 (t, 3H), 3.68 (s, 3H), 3.24 (m, 1H), 2.64 (dd, 1H), 2.52 (dd, 1H), 1.54 (br s, 2H, NH_2). ^{13}C NMR (100.6 MHz, $CDCl_3$, δ from TMS): 174.26 (*C*═O), 144.64, 129.67, 128.04, 126.87, 66.94, 53.89, 52.22, 37.01. FTIR (KBr pellet), ν_{max} (cm^{-1}): 3391 (m, N−H), 3318 (w, N−H), 3062 (w), 2997 (w), 2966 (w), 2948 (w), 2920 (w), 1725 (vs, C═O_{ester}), 1593 (m), 1487 (s), 1446 (s), 1434 (s), 1371 (m), 1348 (m), 1316 (m), 1260 (m), 1205 (s), 1186 (s), 1172 (s), 1095 (m), 1031 (m), 1020 (m), 1001 (m), 952 (m), 892 (w), 854 (m), 838 (m), 810 (m), 771 (m), 747 (s), 705 (s), 676 (m), 665 (m), 630 (m), 615 (s), 530 (w), 508 (m), 494 (m), 474 (m). LRMS-ESI (m/z): $[M + H]^+$ calcd for $C_{23}H_{24}NO_2S$, 378.2; found, 378.2.

Step 2. Boc-Gly-L-Cys(STrit)-OMe. A batch of 4.089 g (10.83 mmol) of H_2N-L-Cys(STrit)-OMe and 2.947 g (10.82 mmol) of Boc-Gly-OSu was combined in 200 mL of CH_2Cl_2 and stirred at room temperature overnight. The solution was then washed with saturated $NaHCO_3$(aq) and brine and dried over $MgSO_4$ before concentration to a white foam solid (4.934 g, 9.228 mmol, 85%). Mp: 59−62 °C. ^{1}H NMR (400 MHz, $CDCl_3$, δ from TMS): 7.44 (d, 6H), 7.33 (t, 6H), 7.26 (t, 3H), 6.80 (br s, 1H, N$H_{peptide}$), 5.38 (br, s, 1H, N$H_{carbamate}$), 4.59 (m, 1H), 3.82 (m, 2H), 3.72 (s, 3H), 2.71 (m, 2H), 1.49 (s, 9H). ^{13}C NMR (100.6 MHz, $CDCl_3$, δ from TMS): 170.70 (C═O_{ester}), 169.31 (*C*═$O_{peptide}$), 155.95 (*C*═$O_{carbamate}$), 144.27, 129.51, 128.03, 126.92, 80.11, 66.98, 52.64, 51.20, 33.67, 28.32. FTIR (KBr pellet), ν_{max} (cm^{-1}): 3320 (br s, N−H), 3057 (m), 3030 (m), 2977 (s), 2952 (m), 2931 (m), 1746 (vs, C═O_{ester}), 1720 (vs, C═$O_{carbamate}$), 1689 (vs, C═$O_{peptide}$), 1595 (w), 1514 (s), 1493 (s), 1434 (m), 1391 (w), 1367 (m), 1248 (m), 1210 (m), 1168 (s), 1083 (w), 1050 (m), 1031 (m), 1001 (w), 985 (w), 941 (w), 862 (w), 766 (m), 744 (s), 701 (s), 675 (m), 621 (m), 544 (w), 505 (w). LRMS-ESI (m/z): $[M + K]^+$ calcd for $C_{30}H_{34}KN_2O_5S$, 573.2; found, 573.0.

Step 3. H_2N-Gly-L-Cys-OMe·TFA (GC-OMeH_2·TFA). A batch of 3.748 g (7.010 mmol) of Boc-Gly-L-Cys(STrit)-OMe was dissolved in 40 mL of a 1:1 CH_2Cl_2/TFA solution resulting in a bright-yellow color. After 30 min, 1.092 g (9.391 mmol) of Et_3SiH was added dropwise to the solution, which bleached the bright-yellow solution to a clear and pale-yellow color. After 90 min of stirring, the solution was concentrated to ~50% of its original volume and the resulting insoluble triphenyl methane byproduct filtered off and washed with TFA. The solution was then concentrated to a pale oil, which solidified upon stirring in Et_2O (1.601 g, 5.228 mmol, 75%). Mp: 74−77 °C. ^{1}H NMR (500 MHz, CD_3CN, δ from protio solvent): 7.86 (br s, 3H, NH_3), 7.62 (s, N$H_{peptide}$), 4.73 (m, 1H), 3.80 (m, 2H), 3.72 (s, 3H), 2.93 (m, 2H), 1.92 (br s, coincides with solvent protio signal, thus difficult to integrate, S*H*). ^{13}C NMR (100.6 MHz, CD_3CN, δ from solvent): 222.35 (*C*═O_{TFA}), 171.02 (*C*═O_{ester}), 167.09 (*C*═$O_{peptide}$), 55.68, 53.21, 41.52, 31.47, 26.74. ^{1}H NMR (500 MHz, D_2O, δ from protio solvent): 4.82 (m, 1H), 3.94 (s, 2H), 3.82 (s, 3H), 3.03 (m, 2H). FTIR (KBr pellet), ν_{max} (cm^{-1}): 3325 (m, N−H), 3138 (br w, N−H), 1753 (s, C═O_{ester}), 1677 (vs, C═$O_{peptide}$), 1631 (w) 1563 (w), 1552 (m), 1536 (w), 1513 (w), 1493 (w), 1434 (m), 1350 (m), 1323 (w), 1208 (s, C−F), 1186 (s, C−F), 1129 (s), 1043 (w), 965 (w), 906 (m), 841 (m), 802 (m), 726 (m), 572 (w). LRMS-ESI (m/z): $[M + H]^+$ calcd for $C_6H_{13}N_2O_3S$, 193.2; found, 193.0.

[Ni_2(GC-OMe)$_2$] (1). *Procedure 1 (TFA Adduct).* To a batch of 0.174 g (0.699 mmol) of $Ni(OAc)_2·4H_2O$ stirring in 12 mL of MeOH was added a 4 mL MeOH solution of GC-OMeH_2·TFA (0.217 g, 0.709 mmol) followed by a 3 mL MeOH solution of NaOAc (0.060 g, 0.731 mmol). The resultant deep orange solution was stirred at room temperature for 16 h, after which the reaction was concentrated to dryness to afford an orange residue. This residue was then stirried in 20 mL of MeCN, which resulted in 0.153 g (0.250 mmol, 72%) of product as peach-colored solids. ^{1}H NMR (400 MHz, D_2O, δ from solvent): 4.28 (m, 1H), 3.96 (s, 3H), 3.49 (dd, 1H), 3.32 (dd, 1H), 2.51 (br, s, 1H), 2.31 (d, 1H), 2.08 (s, 1H), 1.94 (s, 1H). FTIR (KBr pellet), ν_{max} (cm^{-1}): 3420 (w, br, OH), 3246 (m, br, N−H), 3119 (m, br, N−H), 2950 (w), 1729 (s, C═O_{ester}), 1694 (m, C═O_{TFA}), 1601 (vs, C═$O_{peptide}$), 1437 (m), 1409 (s), 1338 (w), 1273 (w), 1205 (s, C−F), 1169 (s, C−F), 1138 (m), 1019 (w), 973 (w), 944 (w), 843 (w), 801 (w), 722 (w), 669 (w), 650 (w), 625 (w), 584 (w), 459 (w). HRMS-ESI (m/z): $[M + H]^+$ calcd for $C_{12}H_{21}N_4Ni_2O_6S_2$ (relative abundance), 496.9604 (100), 497.9637 (13), 498.9559 (88), 499.9591 (11), 500.9515 (22); found, 496.9614 (100), 497.9646 (11), 498.9570 (88), 499.9604 (10), 500.9522 (18). UV−vis (pH 7.5, 50 mM PIPES, 298 K) λ_{max}, nm (ε, M^{-1} cm^{-1}): 338 (4,470), 458 (570). Anal. Calcd for $C_{12}H_{20}N_4Ni_2O_6S_2$·TFA·$2H_2O$: C, 25.95; H, 3.89; N, 8.65. Found: C, 26.13; H, 3.94; N, 8.62.

Procedure 2. To a batch of 1.292 g (5.192 mmol) of $Ni(OAc)_2·4H_2O$ and 0.428 g (5.22 mmol) of NaOAc dissolved in 80 mL of MeOH was added 1.584 g (5.172 mmol) of GC-OMeH_2·TFA in 10 mL of MeOH. The reaction mixture instantly became a deep red-orange color upon addition of ligand and was subsequently heated to 50 °C for 16 h, which resulted in precipitation of product as pink solids. The solids were isolated via vacuum filtration to afford 1.100 g (2.210 mmol, 85%) of product. The isolated product is not readily soluble as is the TFA adduct (see above), but prolonged stirring in D_2O or buffer provided orange solutions with identical spectral properties (^{1}H NMR, UV−vis, ESI-MS). FTIR revealed no TFA peaks. FTIR (KBr pellet), ν_{max} (cm^{-1}): 3326 (w, N−H), 3228 (w, N−H), 3084 (br w, N−H), 2978 (w), 2962 (w), 2929 (w), 1755 (s, C═O_{ester}), 1578 (vs, C═$O_{peptide}$), 1433 (m), 1404 (m), 1360 (m), 1312 (w), 1265 (w), 1200 (m), 1177 (m), 1150 (m), 1114 (m), 1055 (w), 1030 (w), 993 (w), 969 (w), 946 (w), 853 (w), 801 (w), 717 (w), 660 (w), 603 (w), 573 (w), 483 (w), 424 (m). Anal. Calcd for $C_{12}H_{20}N_4Ni_2O_6S_2·0.5H_2O$: C, 28.44; H, 4.18; N, 11.05. Found: C, 28.47; H, 3.94; N, 10.78.

[Ni_2(GC-OMe)$_2$] (1) Prepared in Situ. To a freshly dissolved batch of 18 mg (0.06 mmol) of GC-OMeH_2·TFA in pH 7.5 buffer (50 mM PIPES) was added 15 mg (0.06 mmol) of $Ni(OAc)_2·4H_2O$ to form a richly colored orange solution. All spectral properties are in accordance with those of solid batches of isolated **1** upon dissolution.

K[Ni(GC-OMe)(SC_6H_4-*p*-Cl)] (2). To an 8 mL DMF solution containing 0.142 g (0.777 mmol) of KSC_6H_4-*p*-Cl was added a 5 mL DMF slurry of **1** (0.202 g, 0.406 mmol). The resulting purple heterogeneous mixture was heated to 45 °C and stirred at this temperature for 16 h to form a rich mostly homogeneous violet-colored solution. The reaction was subsequently cooled to room temperature and filtered to remove any unreacted **1**, and the violet mother liquor was concentrated to dryness. The resultant purple residue was then taken up in 2 mL of

THF, which was then precipiated out by addition of 12 mL of Et_2O. The product was collected as dull violet solids via vacuum filtration (0.316 g, 0.732 mmol, 94%). ^{1}H NMR (500 MHz, D_2O, as isolated product in the presence of 1 extra mol-equiv of KSC_6H_4-*p*-Cl, δ from protio solvent): 7.53 (d, 1.4H), 7.30 (d, 1.7H, free KSC_6H_4-*p*-Cl), 7.14 (d, 1.4H), 7.08 (d, 1.7H, free KSC_6H_4-*p*-Cl), 4.15 (m, 1H), 3.79 (s, 3H), 3.31 (dd, 1H), 3.15 (dd, 1H), 2.60 (m, 1H), 2.24 (d, 1H). ^{1}H NMR (400 MHz, CD_3CN, as isolated solid, δ from protio solvent): 7.68 (d, 1.3H), 6.93 (d, 1.1H), 3.84 (m, 1H), 3.61 (s, 2.4H), 3.01 (m, 1H), 2.91 (m, 1H), 2.36 (m, 1H), 2.15 (s, 1H, N*H*), 2.13 (m, 1H), 1.87 (br s, 1H, N*H*). FTIR (KBr pellet), ν_{max} (cm^{-1}): 3325 (w, NH), 3195 (br w, N−H), 3108 (br w, N−H), 2948 (m), 2924 (m), 1722 (s, C═O_{ester}), 1586 (vs, C═$O_{peptide}$), 1468 (s), 1437 (m), 1410 (m), 1336 (w), 1265 (w), 1207 (m), 1168 (m), 1090 (s), 1033 (m), 1010 (m), 934 (w), 818 (m), 740 (w), 701 (w), 662 (w), 543 (m), 499 (w), 425 (w). HRMS-ESI (*m*/*z*): $[M - K]^-$ calcd for $C_{12}H_{14}ClN_2NiO_3S_2$ (relative abundance), 390.9482 (100), 391.9515 (13), 392.9439 (48), 393.9470 (6), 394.9408 (21); Found, 390.9487 (100), 391.9520 (11), 392.9442 (41), 393.9472 (4), 394.9416 (16). UV−vis (DMF, 298 K) λ_{max}, nm (ε, M^{-1} cm^{-1}): 481 (390), 560 (230). UV−vis (pH 7.5, 50 mM PIPES, 298 K) λ_{max}, nm (ε, M^{-1} cm^{-1}): 471 (430), 560 (240). E_{ox} (DMF): 220 mV. E_{ox} (pH 7.4): 285 mV. Anal. Calcd for $C_{12}H_{14}ClKN_2NiO_3S_2 \cdot 0.5H_2O$: C, 32.71; H, 3.43; N, 6.36. Found: C, 32.63; H, 3.56; N, 6.50.

K[Ni(GC-OMe)(S^{t}Bu)] (3). To 115 μL (0.092 g, 1.02 mmol) of *tert*-butyl thiol dissolved in 3 mL of DMF was added 0.040 g (0.997 mmol) of KH as a 4 mL DMF slurry to generate KS^{t}Bu. Immediate effervescence was observed, and a pale yellow homogeneous solution formed over the course of 20 min. To this solution was added a 5 mL DMF slurry of **1** (0.278 g, 0.558 mmol), resulting in a purple heterogeneous mixture. This solution was then heated to 45 °C and stirred for 16 h to form a rich violet-colored solution. The reaction was subsequently cooled to room temperature and filtered to remove any unreacted **1**, and the violet mother liquor was concentrated to dryness. The resultant purple residue was taken up in 6 mL of THF, which was treated with 25 mL of Et_2O to form free-flowing solids. The product was collected as pink solids via vacuum filtration (0.328 g, 0.870 mmol, 87%). ^{1}H NMR (400 MHz, D_2O, as isolated product in the presence of 1 extra mol-equiv of KS^{t}Bu, δ from protio solvent): 4.01 (d, 1H), 3.71 (s, 3H), 3.30 (dd, 1H), 3.14 (dd, 1H), 2.53 (m, 1H), 2.21 (d 1H), 1.26 (s, 9H). ^{1}H NMR (500 MHz, CD_3CN, as isolated solid, δ from protio solvent): 3.70 (m, 1H), 3.59 (s, 3H), 3.04 (m, 1H), 2.95 (m, 1H), 2.30 (m, 1H), 2.13 (m, 1H), 1.84 (s, 2H, N*H*), 1.31 (s, 9H). FTIR (KBr pellet), ν_{max} (cm^{-1}): 3343 (br w, N−H), 3222 (br w, N−H), 3107 (br w, N−H), 2948 (w), 2887 (w), 2848 (w), 1721 (m, C═O_{ester}), 1584 (vs, C═$O_{peptide}$), 1439 (w), 1410 (m), 1355 (w), 1273 (w), 1207 (m), 1166 (m), 932 (w), 742 (w), 646 (w), 586 (w), 465 (w). UV−vis (DMF, 298 K) λ_{max}, nm (ε, M^{-1} cm^{-1}): 358 (1400), 484 (440), 570 (230). E_{ox} (DMF): 80 mV. Anal. Calcd for $C_{10}H_{19}KN_2NiO_3S_2 \cdot H_2O$: C, 30.39; H, 5.36; N, 7.09. Found: C, 30.08; H, 5.02; N, 7.16.

K[Ni(GC-OMe)(SC_6H_4-*p*-OMe)] (4). To a 3 mL DMF solution containing 0.046 g (0.258 mmol) of KSC_6H_4-*p*-OMe was added a 3 mL DMF slurry of **1** (0.073 g, 0.147 mmol). The purple heterogeneous reaction mixture that formed was then heated to 45 °C and stirred for 16 h to form a violet-brown mostly homogeneous solution. The reaction was subsequently cooled to room temperature and filtered to remove any unreacted **1**, and the violet-brown mother liquor was concentrated to dryness. To the resultant red-brown residue was added 5 mL each of THF and Et_2O, and the residue was scraped to form free-flowing solids. The product was collected as red-brown solids via vacuum filtration (0.096 g, 0.225 mmol, 87% yield). ^{1}H NMR (400 MHz, D_2O, as isolated product in the presence of 1 extra mol-equiv of KSC_6H_4-*p*-OMe, δ from protio solvent): 7.37 (d, 2H), 7.21 (d, 2H, free KSC_6H_4-*p*-OMe), 6.72 (m, 4H, overlap of bound and free KSC_6H_4-*p*-OMe), 4.08 (d, 1H), 3.71 (s, 9H, coincidental peaks from: 3H from OMe of coordinated KSC_6H_4-*p*-OMe, 3H from OMe of free KSC_6H_4-*p*-OMe), 3.23 (dd, 1H), 3.07 (dd, 1H), 2.53 (m, 2H). ^{1}H NMR (500 MHz, CD_3CN, as isolated solid, δ from protio solvent): 7.40 (d, 2H), 6.50 (d, 0.3H), 6.41 (d, 1.7H), 3.75 (t, 1H), 3.55 (s, 3H), 3.44 (s, 3H), 2.93 (m, 2H), 2.17 (m, 1H), 2.08 (m, 1H and br s, 1H, N*H*), 1.85 (br s, 1H, N*H*). FTIR (KBr pellet), ν_{max} (cm^{-1}): 3319 (w, N−H), 3190 (br w, N−H), 3090 (br w, N−H), 2946 (w), 2834 (w), 1720 (s, C═O_{ester}), 1663 (m, C═O_{DMF}), 1587 (vs, C═$O_{peptide}$), 1486 (s), 1463 (w), 1439 (m), 1409 (m), 1336 (w), 1273 (m), 1235 (s), 1169 (s), 1099 (m), 1028 (m), 933 (w), 826 (w), 796 (w), 638 (w), 625 (w), 561 (w), 525 (w), 470 (w), 425 (w). HRMS-ESI (*m*/*z*): $[M - K]^-$ calcd for $C_{13}H_{17}N_2NiO_4S_2$ (relative abundance), 386.9978 (100), 388.0011 (14), 388.9933 (48), 389.9965 (7); found, 386.9980 (100), 388.0011 (14), 388.9936 (46), 389.9983 (11). UV−vis (DMF, 298 K) λ_{max}, nm (ε, M^{-1} cm^{-1}): 480 (500), 565 (200). UV−vis (pH 7.5, 50 mM PIPES, 298 K) λ_{max}, nm (ε, M^{-1} cm^{-1}): 467 (400), 550 (230). E_{ox} (DMF): 170 mV. E_{ox} (pH 7.4): 315 mV. Anal. Calcd for $C_{13}H_{17}KN_2NiO_4S_2 \cdot 0.5H_2O$: C, 35.79; H, 4.16; N, 6.42. Found: C, 35.84; H, 4.46; N, 6.48.

K[Ni(GC-OMe)(S-NAc)] (5). To a 5 mL DMF solution containing 0.094 g (0.249 mmol) of **3** was added a 2 mL DMF solution of *N*-acetyl-L-cysteine methyl ester (0.045 g, 0.254 mmol). The solution rapidly changed from violet to orange-brown and was left to stir at room temperature for 16 h. The solution was then concentrated to a brick-red colored residue and stirred in 15 mL of a 2:1 Et_2O/THF mixture to afford free-flowing solids. The solids were collected via vacuum filtration to yield 0.105 g (0.226 mmol, 91% yield) of product. ^{1}H NMR (400 MHz, D_2O, as isolated product in the presence of one extra mol-equiv of KS-NAc, δ from protio solvent): 4.45 (t, 1H, free KSNAc), 4.32 (t, 1H), 4.11 (d, 1H), 3.73 (s, 6H, coincidental peaks: 3H each from OMe of coordinated $[GC\text{-}OMe]^{2-}$ and $[S\text{-}NAc]^-$, 3H from OMe of free KS-NAc), 3.31 (dd, 1H), 3.17 (dd, 1H), 2.86 (m, 2.5H, free KSNAc), 2.63 (m, 1H), 2.26 (d, 1H), 2.14 (m, 2H), 2.08 (s, 3H), 2.02 (s, 4H, free KSNAc). ^{1}H NMR (500 MHz, CD_3CN, as isolated solid, δ from protio solvent): 8.62 (br s, 1H, N*H*), 4.05 (br s, 1H), 3.90 (br s, 1H), 3.60 (s, 8H, coincidental peaks from: OMe of both coordinated $[GC\text{-}OMe]^{2-}$ and $[SN\text{-}Ac]^-$, residual THF from reaction workup), 3.32 (br s, 1H), 3.05 (m, 1H), 2.97 (m, 1H), 2.51 (m, 1H), 2.14 (m, 10H, integrates slightly high due to overlap with residual H_2O peak). FTIR (KBr pellet), ν_{max} (cm^{-1}): 3246 (br w, N−H), 2950 (w), 2919 (w), 2848 (w), 1731 (s, C═O_{ester}), 1662 (s, C═$O_{SNAC\ peptide}$), 1589 (vs, C═$O_{GCOMe\ peptide}$), 1436 (m), 1412 (m), 1372 (w), 1337 (w), 1302 (w), 1268 (w), 1212 (m), 1167 (m), 1122 (w), 1032 (w), 938 (w), 901 (w), 843 (w), 800 (w), 661 (w), 567 (w), 488 (w), 423 (w). HRMS-ESI (*m*/*z*): $[M - K]^-$ calcd for $C_{12}H_{20}N_3NiO_6S_2$ (relative abundance), 424.0142 (100), 425.0174 (13), 426.0097 (48), 427.0129 (6), 428.0072 (5); Found, 424.0144 (100), 425.0180 (12), 426.0101 (48), 427.0135 (6), 428.0081 (4). LRMS-ESI (*m*/*z*): $[M - K]^-$ calcd for $C_{12}H_{20}N_3NiO_6S_2$, 424.0; found, 424.0. UV−vis (DMF, 298 K) λ_{max}, nm (ε, M^{-1} cm^{-1}): 358 sh (1,200), 463 (350), 545 (160). UV−vis (pH 7.5, 50 mM PIPES, 298 K) λ_{max}, nm (ε, M^{-1} cm^{-1}): 334 (1,200), 464 (300), 545 (140). E_{ox} (DMF): 310 mV. E_{ox} (pH 7.4): 550 mV. Anal. Calcd for $C_{12}H_{20}KN_3NiO_6S_2 \cdot 0.33THF \cdot 0.33H_2O$: C, 32.40; H, 4.76; N, 8.50. Found: C, 32.46; H, 4.80; N, 8.67.

Bulk Oxidation of 2. To a batch of 52 mg (0.12 mmol) of **2** in 3 mL of DMF was added 40 mg (0.12 mmol) of ferrocenium hexafluorophosphate in 3 mL of DMF. Instantaneously, the violet solution developed an orange-brown color and was left to stir at room temperature for 2 h. The reaction mixture was then concentrated to an orange-brown residue, which solidified upon stirring in Et_2O. Brown solids (45 mg) were separated via vacuum filtration, and the yellow mother liquor was concentrated to a pale yellow residue (40 mg). FTIR (KBr), ^{1}H NMR (D_2O), and ESI-MS (positive ion mode) revealed the brown insoluble solids to be comprised of **1** and KPF_6 (87% recovery), while ^{1}H NMR in $CDCl_3$ of the yellow Et_2O-soluble residue was revelead to be comprised

dx.doi.org/10.1021/ic2016462 |*Inorg. Chem.* 2011, 50, 10460–10471

Scheme 2. Synthesis of GC-OMeH$_2$

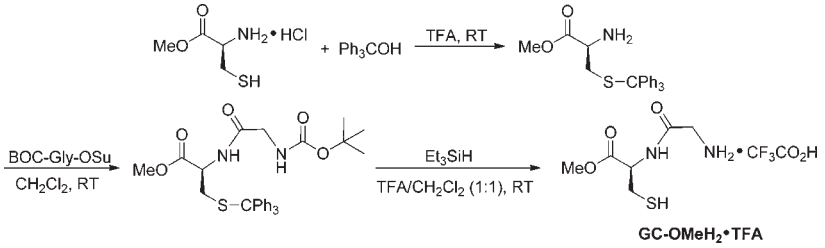

solely of ferrocene and the disulfide of the thiol HSC_6H_4-*p*-Cl (100% recovery).

X-ray Absorption Studies. Samples were loaded under anaerobic conditions into 0.5 mm thick XAS aluminum sample holders with Mylar-tape windows and quickly frozen in liquid nitrogen prior to XAS data collection. Nickel K-edge XAS data were collected at the Stanford Synchrotron Radiation Lightsource (SSRL) on beamline 7−3 with the SPEAR storage ring operating at 3.0 GeV, 345−350 mA. X-ray absorption spectra for the solid samples were recorded with the sample at 10 K using a 1 mm × 4 mm vertical aperture beam incident on a fully tuned Si[220] double-crystal monochromator and collected using transmission mode. Three ionization chambers with N_2 gas were used with the first defining I_0. A nickel foil was placed between the second and the third ionization chambers I_1 and I_2 to serve as an internal calibration standard with the first inflection point for the nickel foil assigned at 8331.6 eV. *k* values were calculated using a threshold ($k = 0$) energy of 8340 eV. The averaged XAS data for a solid sample represent 5−6 scans, each of 27 min duration; the averaged spectra were calculated as $\log(I_0/I_1)$. Data reduction and analysis were performed with EXAFSPAK software (www-ssrl.slac.stanford.edu/exafspak.html) according to standard procedures as described before.[57] Fourier transforms of the EXAFS spectra were generated using sulfur-based phase correction. Phase and amplitude functions used in the curve fitting were calculated using FEFF version 8.0.[58]

RESULTS AND DISCUSSION

Synthesis. In constructing accurate structural and functional models of Ni−SOD, certain design elements must be considered. First, the ligand frame must contain a mixed N/S donor set to mimic the coordination sphere observed in the enzyme. Second, and beyond a mere stoichiometric replication of the donor atoms, is the electronic nature of the N/S frame which should contain one peptide-N (carboxamide-N is the more general terminology), one primary amine-N, and two *cis*-thiolates situated in a planar N_2S_2 arrangement. An additional imidazole-N ligand would be required to replicate the four-coordinate to five-coordinate Ni(II/III)−SOD redox conversion. Third, the ligand construct should be amenable to a variety of straightforward modifications. This important last requirement will permit for electronic and structural "fine tuning" of the biomimetic for its desirable function. Several groups have achieved some or all of these criteria by employing (i) small peptides or peptide maquettes typically 3−12 amino acids long,[27−30,33,34] (ii) symmetric N_2S_2 frames that approximate the electronic nature of the Ni−SOD donors,[40,41,59] (iii) electronically accurate N_2S_2 frames,[35,36] (iv) asymmetric N_2S ligands that approximate the Ni active site with an open coordination site where exogenous N-donors bind (NiN_3S),[60,61] and (v) asymmetric N_2S ligands with Ni−SOD accurate donors containing an open coordination site where exogenous S-ligands bind to afford NiN_2S_2 species.[38,39] In this work we utilized design methodologies from i and v (see previous) resulting in the Gly-Cys N_2S ligand that we denote as GC-OMeH$_2$. We hypothesized that GC-OMeH$_2$ would provide water-soluble small-molecule Ni−SOD biomimetics that model the *exact basal plane contributions* of His1 and Cys2 in the enzyme. Simultaneously, via strategies developed by our group, a fourth and exchangeable coordination site amenable to synthetic fine tuning is left available by which monodentate thiolate ligands (modeling the Cys6 contribution in Ni−SOD) can be appended.

Synthesis of GC-OMeH$_2$ occurred in three steps by standard peptide coupling routes that provided the final ligand in high yield (Scheme 2). Protection of the thiol group of L-cysteine methyl ester occurred in 81% yield by reaction of the amino acid with triphenylmethanol (trityl protection) in TFA. Formation of the pre-ligand is achieved by coupling of the protected cysteine methyl ester with BOC-Gly-OSu, resulting in the S-trityl-protected ligand in 85% yield. Finally, deprotection of the trityl and BOC groups with Et_3SiH in a TFA/CH_2Cl_2 (1:1) mixture furnished the TFA adduct of GC-OMeH$_2$ in 74% yield. The ligand is a white solid material that is thermally stable even in aerobic conditions.

The monomeric Ni(II)−N_2S_2 complexes originate from the dimeric species, [Ni$_2$(GC-OMe)$_2$] (**1**), which is isolated in high yield by reaction of $Ni(OAc)_2 \cdot 4H_2O$ with ligand and 1 molequiv of NaOAc in MeOH at room temperature, resulting in orange-colored solutions. TFA still seems to be associated with **1** depending on the reaction conditions, which has been confirmed by FTIR and elemental analysis (see Experimental Section). These peach-colored solids have been formulated as an aquated TFA species, namely, $\mathbf{1} \cdot TFA \cdot 2H_2O$, according to microanalysis. Heating MeOH solutions of $\mathbf{1} \cdot TFA \cdot 2H_2O$ to 50 °C for 16 h resulted in precipitation of analytically pure [Ni$_2$(GC-OMe)$_2$] (**1**) as pink solids with no evidence of TFA peaks in the IR spectrum. Complex **1** is generally insoluble in both polar and non-polar solvents, a property consistent with previously isolated dimeric S,S′-bridged $Ni_2(N_2S)_2$ complexes;[38,39] however, stirring in water resulted in slow dissolution to afford orange solutions with a spectral profile identical to that obtained via the spontaneous metalation of GC-OMeH$_2$ · TFA with Ni(II) in pH 7.5 PIPES buffer. ESI-MS$^+$ analysis of **1** also revealed the presence of species corresponding to [Ni$_2$(GC-OMe)$_2$ + H]$^+$ (**1** + **H**), [Ni$_3$(GC-OMe)$_3$ + H]$^+$, and [Ni$_4$(GC-OMe)$_4$ + H]$^+$, suggesting that various permutations of 1:1 Ni/GC-OMe stoichiometry may exist upon dissolution (Figures S17−19, Supporting Information). Regardless, ^{1}H NMR studies in D_2O revealed a chemical equivalency throughout any species which may be present (vide infra). It should be noted that deprotonation of ligand protons with a strong base such as NaH in an aprotic solvent (MeCN) resulted in formation of intractable

dx.doi.org/10.1021/ic2016462 |*Inorg. Chem.* 2011, 50, 10460–10471

brown solids upon addition of Ni(II); the exact nature of such species is unknown at present, but FTIR revealed loss of the GC-$OMeH_2$ ester functionality, suggesting that the coordination chemistry of GC-$OMeH_2$·TFA with Ni(II) is relatively facile in polar protic solvents and a strong base is not required.

Despite its unfavorable solubility properties, complex **1** is a good metallosynthon for preparation of the monomeric Ni(II) complexes **2**−**5** via addition of 2 mol-equiv of the appropriate potassium thiolate salts to DMF solutions of **1** heated to 45 °C (Scheme 3) (where SC_6H_4-*p*-Cl = thiolate of *p*-chlorobenzene thiol; S^tBu = thiolate of *tert*-butylthiol; SC_6H_4-*p*-OMe = thiolate of *p*-methoxybenzenethiol; SNAc = thiolate of *N*-acetyl L-cysteine methyl ester). The S,S′-bridge-splitting reactions to form **2**−**4** resulted in high yields of the complexes (87−90%). As reported by our group, complexes of general formula $[Ni(N_2S)(SR)]^-$ can be synthesized several ways: (i) S,S′-bridge-splitting of Ni dimer (similar protocols have been utilized by Holm[62] and Darensbourg[60]); (ii) pK_a-driven thiol exchange; and (iii) a disulfide/coordinated thiolate redox exchange procedure.[38,39] These alternate methodologies have been successfully applied to this generation of water soluble Ni−SOD mimics. For example, complex **5** was obtained in 90% yield via addition of 1 mol-equiv of HSNAc to **3** in DMF. Complex **2** was also prepared from **3** utilizing 0.5 mol equiv of the disulfide of HSC_6H_4-*p*-Cl. These facile reactions to obtain monomeric Ni(II) species demonstrate the efficacy of these preparations when applied to different ligand systems that may be applied to future Ni−SOD models.

PROPERTIES

General. Complexes **1**−**5** are stable in anaerobic aqueous solutions for up to 16 h as monitored by ^{1}H NMR. No evidence of ligand protonation, dissociation, or metal-mediated ester hydrolysis is observed which is in contrast to other reported $Ni(II)N_2S_2$ complexes.[63] UV−vis spectral monitoring of complexes **2**, **4**, and **5** in pH 7.5 buffer (PIPES) revealed slight increases in the intensity of λ_{max} over prolonged time periods (>6 h) due to light scattering as these solutions became cloudy. The dimeric complex **1** is air stable in solution over 16 h as evidenced by ^{1}H NMR and UV−vis, consistent with the stability brought about by S,S′-bridging. Collectively, solutions of **2**−**5** are relatively air stable and can be handled aerobically without significant decomposition on the hour time scale. However, prolonged aerobic storage resulted in color bleaching and cloudiness for periods of extended exposure (>6 h).

Scheme 3. Synthesis of Ni(II) Complexes 2−5

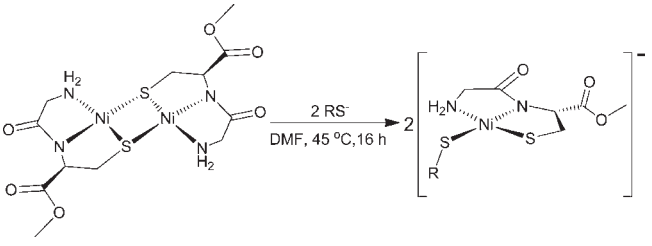

Infrared. FTIR spectra of metal−peptide complexes serve as good indicators for peptido-N → M binding from the observed red-shift in ν_{CO} of the carbonyl peptide. This noted shift is observed in **1**−**5** with ν_{CO} frequencies between 1578 and 1589 cm^{-1} (KBr matrix), which red-shifted ∼100 cm^{-1} from the free ligand (ν_{CO} 1677 cm^{-1} in KBr) and confirmed formation of the peptido-N → M bond. In general, ν_{CO} appeared to be invariant, regardless of the donor strength of the monodentate thiolate ligand trans to the peptido-N. In fact, the lowest energy ν_{CO} stretch was observed for **1** despite the bridging nature of the coordinated thiolates. As expected, ν_{NH} of the peptide-N was absent in the Ni(II) complexes. Coordination of the $-NH_2$ functionality in **1**−**5** was also evident as the ν_{NH} stretches appeared at values from 3042 (**5**) to 3108 cm^{-1} (**2**) compared to ν_{NH} of the free ligand (3318 cm^{-1}). In general, ν_{NH} of organic primary amines occurs at values ≥3250 cm^{-1}.[64]

^{1}H NMR and ESI-MS. ^{1}H NMR spectra of **1**−**5** reveal that these Ni(II) complexes are d^8 square-planar systems in solution (D_2O and CD_3CN at 298 K) as evident by their spectra, which are typical for diamagnetic ($S = 0$) molecules. For example, the D_2O ^{1}H NMR spectrum of dimer **1** revealed only one signal per non-equivalent proton, indicative of an electronically identical environment per Ni(II) with respect to GC-OMe^{2-} protons. In contrast, the D_2O ^{1}H NMR spectra of as-isolated **2**−**5** display broad, ill-resolved signals indicative of an equilibrium mixture of Ni(II) species likely due to loss of the exogenous RS^- ligand and formation of $[Ni_x(GC\text{-}OMe)_x(SR)]$ or $[Ni(GC\text{-}OMe)(OH_2)_x]$-type species (Scheme 4). The precise nature of the species present upon dissolution of the as-isolated complexes is unknown, but the spectra suggest more than one which may be oligomeric in nature. When 1 mol-equiv of the corresponding thiolate is added to these D_2O solutions, however, the NMR spectra became well resolved with defined peaks that are consistent with monomeric ($S = 0$) $[Ni(GC\text{-}OMe)(SR)]^-$ complexes (Figure 1 for **2**, see the Supporting Information for **3**−**5**). ESI-MS^- analysis of as-isolated **2** and **4** dissolved in protic solvents revealed ions corresponding to $[Ni_2(GC\text{-}OMe)_2(SR)]^-$, $[Ni_3(GC\text{-}OMe)_3(SR)]^-$, and $[Ni_4(GC\text{-}OMe)_4(SR)]^-$ in addition to those of the parent ion (Figures S20−25, Supporting Information). Similarly, $[Ni_2(GC\text{-}OMe)_2(SNAc)]^-$ is observed along with the parent ion for **5**. The $^tBuS^-$ ligand of complex **3** dissociated completely at pH

Scheme 4. Equilibrium Distribution of Speculative $[Ni_x(GC\text{-}OMe)_x(SR)]$ Species (where $x = 2-4$) Present upon Dissolution of As-Isolated 2−5 in pH 7.5 PIPES Buffer at 298 K[a]

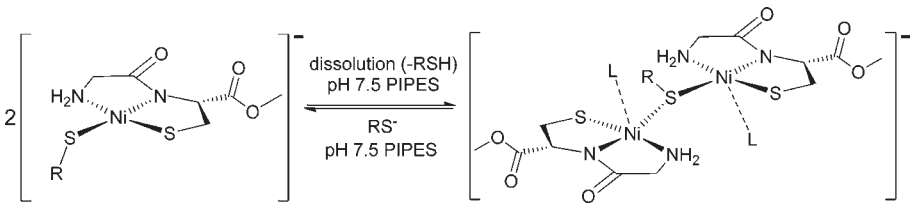

[a] L is a generic ligand potentially representative of solvent or other [Ni(GC-OMe)] fragments.

dx.doi.org/10.1021/ic2016462 |Inorg. Chem. 2011, 50, 10460–10471

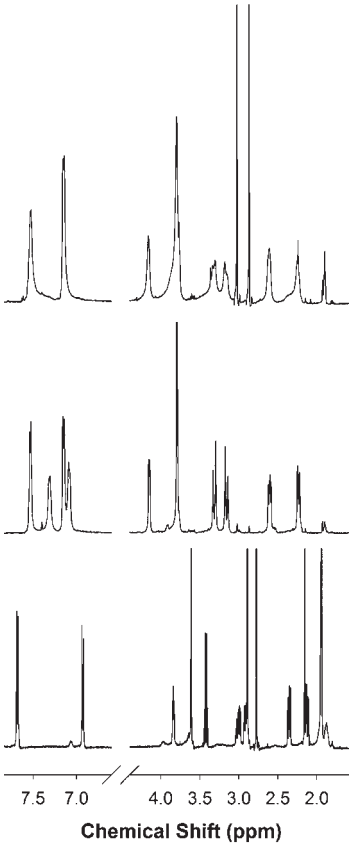

Figure 1. ^{1}H NMR spectrum of **2** recorded under different conditions at 298 K. (Top) As-isolated **2** in D_2O (signals at 3.01 and 2.85 ppm correspond to associated DMF). (Middle) Complex **2** in D_2O after addition of 1 mol-equiv of KSC_6H_4-*p*-Cl (doublets at 7.41 and 7.19 correspond to non-coordinated KSC_6H_4-*p*-Cl). (Bottom) As-isolated **2** in CD_3CN (signal at 3.42 corresponds to Et_2O present in the sample; 2.89 and 2.77 correspond to associated DMF; 1.94 arises from residual protio solvent).

7.5, affording orange-colored solutions that are consistent with reformation of dimer **1**. However, addition of 1 mol-equiv of KS^tBu in D_2O reestablished the violet monomer (vide infra). Furthermore, neither the parent ion of **3** or any species of formula $[Ni_x(GC\text{-}OMe)_x(S^tBu)]^-$ is observed in the ESI-MS. These results suggest a dynamic situation involving potential S-bridging interactions, loss of monodentate thiolate, and possible aquation/solvation for **2**−**5** in H_2O and other protic media (Scheme 4). It is not too surprising that an equilibrium exists with these peptide ligands as a nonapeptide Ni−SOD maquette analogue has been shown to exist in equilibrium with a 2:1 Ni/peptide and 1:1 Ni/peptide species in solution via UV−vis titrations.[31] However, ESI-MS measurements reveal a 1:2 Ni/peptide ratio with a considerable amount of free peptide. These seemingly contradictory results clearly establish that in the absence of the Ni−SOD protein matrix the probability of multiple Ni−L species (where L is a generic representation of any peptido-N/thiolato-S ligand of denticity ≤ 3) is high at least in water. In fact, site-directed mutagenesis of the Cys-S ligands of Ni−SOD suggest that even mutation of one cysteine to serine promotes a high-spin (S = 1) octahedral Ni(II) site with no S-ligands (replaced by H_2O).[22,24] To support this proposal, the ^{1}H NMR spectra of as-isolated **2**−**5** in CD_3CN show no evidence of such behavior and display clean spectra consistent with the diamagnetic square-planar $[Ni(GC\text{-}OMe)(SR)]^-$ formulation (Supporting Information). Thus, the as-isolated Ni(II) monomeric complexes remain fully intact in polar aprotic solvents, which further support the notion that the equilibrium is promoted by interaction with solvent protons and thiolate dissociation.

Electronic Absorption Spectroscopy. The UV−vis spectra of **2**−**5** in DMF or pH 7.5 buffer (PIPES) at 298 K display two predominant features in the visible region (∼470 and 550 nm) (Figure 2, Table 1), which are consistent with the red-violet color of these solutions and similar in nature to Ni−SOD_{red}.[23] In DMF, the most intense visible band is broad and ranges from 463 nm (ε = 350 M^{-1} cm^{-1}) for **5** to 484 nm (ε = 440 M^{-1} cm^{-1}) for **3**; similar visible transitions are observed in Ni−SOD_{red} at 450 nm (ε = 480 M^{-1} cm^{-1})[23] and other square-planar Ni(II)N_2S_2 complexes.[35,36,65−71] These absorptions are proposed to be ligand-field (d−d) transitions containing a minor charge-transfer (CT) contribution.[23] A second less intense ligand-field band appears as a shoulder between 545 nm (ε = 160 M^{-1} cm^{-1}) for **5** and 570 nm (230 M^{-1} cm^{-1}) for **3** and mirrors a similar feature in Ni−SOD_{red} at 543 nm (ε = 150 M^{-1} cm^{-1}). The high-energy band at 361 nm (ε = 880 M^{-1} cm^{-1}) in Ni−SOD_{red} is also observed in **3** (λ_{max} = 358 nm; ε = 1400 M^{-1} cm^{-1}) and **5** (λ_{max} = 358 nm; ε = 1200 M^{-1} cm^{-1}) further underscoring the electronic structural similarities between our models and the enzyme (Figure S1, Supporting Information). The same high-energy feature is difficult to elucidate in **2** and **4** due to the presence of an overwhelming transition in the UV, presumably $\pi-\pi^*$ in nature. UV−vis spectra of **2**, **4**, and **5** in buffer do not differ much from those in DMF (Figure 2, Table 1), suggesting that the various Ni(II) species present retain $GC\text{-}OMe^{2-}$ ligation. For example, λ_{max} = 471 nm (ε = 430 M^{-1} cm^{-1}) for **2** and 458 nm (ε = 570 M^{-1} cm^{-1}; 285 M^{-1} cm^{-1}/Ni) for **1**. Similarly, the less intense feature at 545 nm (ε = 140 M^{-1} cm^{-1}) for **5** and 560 nm (ε = 240 M^{-1} cm^{-1}) for **2** is somewhat less pronounced than in the DMF samples. Higher energy transitions at $\lambda_{max} \approx$ 338 nm are also present for **1** and **5** (Figure S2, Supporting Information). Interestingly, dissolution of **3** in buffer provides a spectral profile identical to dimer **1**, suggestive of protonation and loss of the more basic $^tBuS^-$ ligand.

Since the aqueous electronic absorption spectra of as-isolated **2**, **4**, and **5** represent an equilibrium mixture of Ni(II) species we also recorded their spectra in the presence of excess thiolate to generate one monomeric species (see NMR discussion above). When 1 mol-equiv of KSC_6H_4-*p*-Cl, KSC_6H_4-*p*-OMe, and HSNAc are added to as-isolated buffered solutions of **2**, **4**, and **5**, respectively, only subtle changes in the visible region of the UV−vis spectra resulted (Figures S26−28, Supporting Information). For example, the lowest energy ligand-field shoulder between 545 and 560 nm becomes more pronounced for all complexes. As discussed above, **3** forms dimer **1** when dissolved in buffer. Even addition of up to 5 mol equiv of KS^tBu to as-isolated **3** afforded no change in the UV−vis. Interestingly, addition of 1 mol equiv of HSNAc to **5** resulted in loss of the 334 nm band (Figure S28, Supporting Information) that likely originates from **1** or a species of high nuclearity, suggesting a similar dissociation process may also occur in **5**. Collectively, these results suggest that the Ni(II) species present upon dissolution of as-isolated **2**, **4**, and **5** in buffer are electronically similar to the formally monomeric species that form in the presence of excess RS^-.

dx.doi.org/10.1021/ic2016462 |*Inorg. Chem.* 2011, 50, 10460–10471

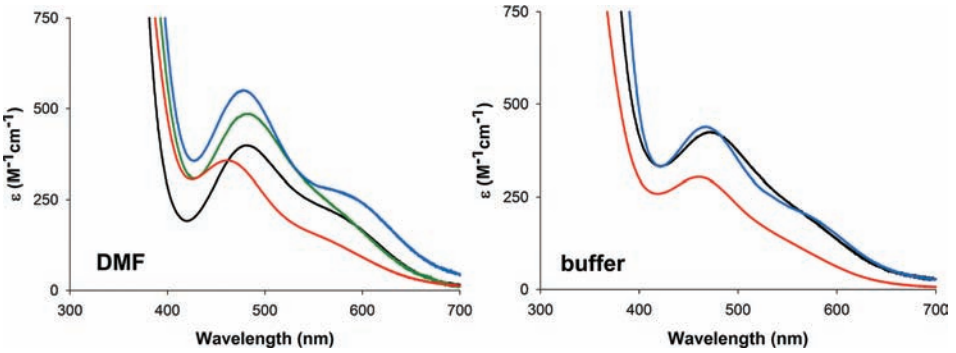

Figure 2. Electronic absorption spectra for **2** (black), **3** (green), **4** (blue), and **5** (red) in DMF (left) and of **2**, **4**, and **5** (same color scheme) in pH 7.5 PIPES buffer (right) recorded at 298 K.

Table 1. Spectroscopic (UV−vis) and Electrochemical (CV) Properties of 2−5 in the Listed Solvents in Comparison to Ni−Peptide Maquettes and Ni−SOD_{red}

complex	λ_{max}, nm (ε, M^{-1} cm^{-1}) in DMF	λ_{max}, nm (ε, M^{-1} cm^{-1}) in buffer	E (V vs Ag/AgCl) in DMF	E (V vs Ag/AgCl) in buffer	ref
2[a]	481 (390)	471 (430)	0.220	0.285	this work
	560 (230)	560 (240)			
3[a]	484 (440)	N/A[e]	0.080	N/A[e]	this work
	570 (230)				
4[a]	480 (500)	467 (400)	0.170	0.315	this work
	565 (200)	550 (230)			
5[a]	463 (350)	464 (300)	0.310	0.550	this work
	545 (160)	545 (140)			
[Ni(SOD^{M1})][b]	N/A	458 (510)	N/A	0.700	28
		552 (240)			
[Ni(SOD^{M2})][c]	N/A	457 (345)	N/A	0.520	29
		548 (130)			
Ni−SOD_{red}[d]	N/A	450 (480)	N/A	0.487	22,24
		543 (150)			

[a] UV−vis and CV (E_{ox} reported) recorded at 298 K; spectra recorded in pH 7.5 PIPES buffer; CV recorded in pH 7.4 phosphate buffer. [b] M1 = H_2N-HCDLPCGVYDPA-CO_2H;[28] UV−vis and CV recorded at room temperature in pH 7.2 phosphate buffer (quasi-reversible $E_{1/2}$ reported on a sample immobilized as a thin film; 0.1 M NaCl electrolyte). [c] M2 = H_2N-HCDLPCG-CO_2H;[30] UV−vis and CV recorded at room temperature in pH 7.4 NEM buffer (quasi-reversible $E_{1/2}$ reported on a sample immobilized as a thin-film; 0.1 M $NaClO_4$ electrolyte).[30] [d] Redox titration recorded at room temperature in pH 7.5 phosphate buffer ($E_{1/2}$ originally referenced versus NHE = 0.290 V).[25] [e] Complex **3** reverts to dimer **1** in aqueous solutions (see the main text).

The similarities between the electronic absorption spectra of **1**−**5** and Ni−SOD_{red} suggest that our models successfully reproduce the electronic environment of the NiN_2S_2 unit in the enzyme active site (Figure 2, Table 1). One interesting point to note when comparing spectra obtained in DMF and buffer is that the ligand-field transitions of **2** and **4** blue shift ∼10 nm in buffer; however, complex **5** does not shift at all. An attractive explanation is that the peptide-NH of the $SNAc^-$ ligand forms an intramolecular H-bond with the thiolato-S ligands in DMF in a manner approximating aqueous H-bonding interactions.[38] The observation that δ_{NH} shifts by >1 ppm downfield in the ^{1}H NMR (8.62 ppm in CD_3CN) of the tethered peptide of $SNAc^-$ in **5** (Supporting Information) compared to δ_{NH} of free HSNAc (7.43 ppm) supports the presence of intramolecular H-bonding interactions. Prior experimental and theoretical investigations pertaining to $SNAc^-$ bound to the Ni(nmp) synthon also corroborate this notion.[38] Furthermore, spontaneous loss of the ^{t}BuS^- ligand from **3** in buffer provides supporting evidence for interaction of the coordinated thiolates with solvent protons in these systems.

Electrochemistry. Cyclic voltammetry (CV) measurements in DMF show irreversible oxidation (E_{ox}) events for **2**−**5** (Figure 3, Table 1). Irreversible CVs have been typical for a number of Ni(II)−N_2S_2 SOD models[35,36,38,39] and indicate an overall change in the coordination environment after oxidation, most likely a result of a thiolate−disulfide conversion, which is prevented in the enzyme. Comparison of the potentials demonstrated patterns which can be roughly correlated to the donor strength of the monodentate RS^- ligand. For example, E_{ox} for the reported complexes increase (more difficult to oxidize) in the following order: **3** (0.080 V vs Ag/AgCl) < **4** (0.170 V) < **2** (0.220 V) < **5** (0.310 V). This observation corresponds well with the trend established using the Ni(nmp) synthon where redox potentials of [Ni(N_2S)(SR)]$^-$ complexes increase as the donor strength of the exogenous RS^- decreases when separately analyzing aryl- and alkyl-SR ligands.[38] As observed in the UV−vis, complexes featuring alkyl RS^- donors tend to be more sensitive to electronic perturbations such as intramolecular H-bonding and solvent environment. In pH 7.4 buffer (phosphate) E_{ox} follows **2** (0.285 V vs Ag/AgCl) < **4** (0.315 V) < **5** (0.550 V)

dx.doi.org/10.1021/ic2016462 |Inorg. Chem. 2011, 50, 10460–10471

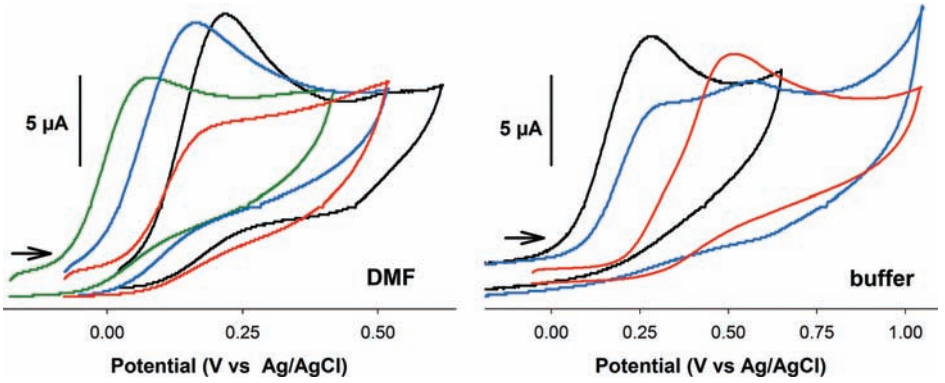

Figure 3. (Left) Cyclic voltammograms (CVs) of 5 mM solutions of **2** (black), **3** (green), **4** (blue), and **5** (red) (vs Ag/Ag^+ in DMF, 0.1 M $^nBu_4NPF_6$ supporting electrolyte, glassy carbon working electrode, scan rate 100 mV/s, room temperature). (Right) CVs of 5 mM solutions of **2**, **4**, and **5** (vs Ag/AgCl in pH 7.4 phosphate buffer, 0.5 M KNO_3 supporting electrolyte, glassy carbon working electrode, scan rate 100 mV/s, room temperature). The CV of **5** in buffer was scaled down (33%). Arrow indicates direction of scan.

(Figure 3, Table 1). Comparing **2** and **4**, it is evident that the more positive redox event belongs to the complex with the more strongly donating RS^-. Among the alkyl RS^- no comparison is available due to spontaneous dissociation of $^tBuS^-$ from **3** in buffer (**1** shows no redox waves up to +1.00 V). In fact, a second E_{ox} is observed in the CV of **4** at 0.480 V, which was found to match that of KSC_6H_4-*p*-OMe dissolved in the same buffer and suggests that the facile RS^- dissociation observed in **3** occurs in **4** as well albeit to a lesser magnitude. The RS^- protonation/dissociation observed in buffer points toward strong interactions between RS^- and solvent protons. The appearance of such an interaction is expected to increase with increasing RS^- basicity and serves to rationalize the reverse trend in E_{ox} of **2** and **4** as well as the observed dissociation of the more basic thiolates. In accordance with this hypothesis, shifts of 0.065, 0.145, and 0.220 V to more positive potentials are observed for **2**, **4**, and **5**, respectively, when comparing the potentials obtained in buffer to those in DMF; a trend which also correlates to relative RS^- basicity.

The E_{ox} values for **2**−**5** arise at potentials which are distinct from those obtained for free ligand and the K^+ salts of their respective RS^- ligands in both DMF and buffer, supporting the notion that the redox-active species present are indeed the Ni(II) complexes and not dissociated RS^-. It should also be noted that addition of 1 mol-equiv of the appropriate RS^- or RSH ligand to solutions of the as-isolated complexes provided no change in E_{ox}, consistent with the aforementioned observation (UV−vis, above) that the species present upon dissolution of as-isolated **2**, **4**, and **5** in aqueous buffer are electronically similar to the corresponding discrete monomeric species. The recorded E_{ox} values also fall between the 0.04 and 1.09 V (vs Ag/AgCl) potential window defined by the two SOD half reactions[72] and imply that these complexes are thermodynamically poised for at least one turnover. However, the irreversible nature of the CV demonstrates that the Ni(III) state obtained during catalysis in the enzyme is not stabilized in these models. Not surprisingly, few Ni−SOD peptide maquettes or small-molecule analogues have ever been isolated in the corresponding Ni(III) state and attempts at chemical oxidation resulted in complex degradation, most likely via disulfide formation.[29] In fact, disulfide formation of the coordinated monodentate thiolate in **2**, **4**, and **5** appear to be responsible for the reported E_{ox}. Bulk oxidation of **2** with 1 mol-equiv of a ferrocenium salt afforded **1** and the disulfide of *p*-chlorobenzene thiol in quantitative yield. Accordingly, these complexes provide no protection against superoxide reduction of *p*-nitroblue tetrazolium chloride (NBT) to its ring-open formazan form in the presence of 25 mol-equiv of KO_2.[73] It should be noted that addition of up to 10 mol-equiv of an exogenous N-donor such as imidazole (Im) imparted no SOD activity, electrochemical reversibility as measured by CV, or changes in the UV−vis spectrum, suggesting no affinity of the Ni center in these systems for Im.

X-ray Absorption Spectroscopy (XAS). Although single crystals of the Ni−peptide complexes were not obtained, we were able to obtain limited structural information on these systems through Ni K-edge X-ray absorption spectroscopy (XAS). The XAS acquired for complexes **2** and **5** reveal Ni(II) systems with an approximately square-planar coordination geometry about the metal center. The XANES area of the spectrum confirmed this assignment as each complex displays an intense pre-edge peak corresponding to a $1s \rightarrow 4p_z$ transition at ~8336 eV (see Figure 4 and Table 2), which is characteristic of Ni(II) in D_{4h} (square-planar) symmetry.[74,75] For comparison, XAS were acquired on members of the crystallographically characterized $[Ni(nmp)(SR)]^-$ family of complexes, which also afford edge features similar to **2** and **5** as further confirmation of the square-planar nature of the systems reported here. The EXAFS region of **2** and **5** are best fit with two non-equivalent Ni−N scatterers at 1.83(3) and 1.96(3) Å, which we assign as $Ni-N_{peptide}$ and $Ni-N_{amine}$, respectively, based on EXAFS of the Ni(nmp) complexes (see Table 2 and the Supporting Information). To complete the NiN_2S_2 coordination sphere, two Ni−S scatterers are also observed at an average distance of 2.16(2) Å. These distances compare well with other $Ni-N_2S_2$ SOD models,[35,36,38,39] peptide maquettes,[29] and the enzyme itself.[18−20] The XAS thus complement the UV−vis, ESI-MS, and ^1H NMR studies and reveal that the reported Ni(II)−peptide complexes are excellent structural and spectroscopic analogues of $Ni-SOD_{red}$.

Relationship to Ni−SOD. Ligand substitution in square-planar d^8 complexes generally follow an associative or interchange pathway where a five-coordinate (5C) trigonal bipyramidal intermediate is invoked in the transition state.[66] In the present systems, one may assume a 5C intermediate is traversed (and may be stabilized) during spontaneous RS^- dissociation in aqueous buffer. Formation of a higher coordination number species would explain the broadness in the ^1H NMR spectra due to potential Ni(II) $S = 1$ solvated derivatives that form once the

dx.doi.org/10.1021/ic2016462 |*Inorg. Chem.* 2011, 50, 10460–10471

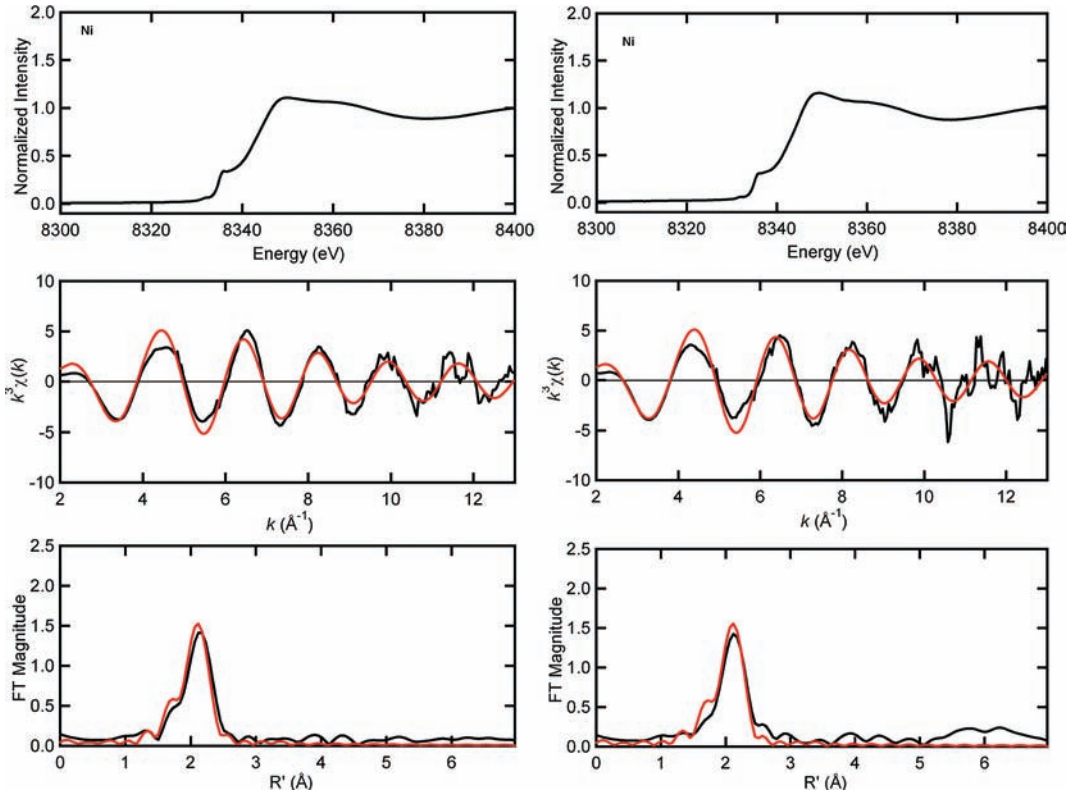

Figure 4. Ni K-edge X-ray absorption data for K[Ni(GC-OMe)(S-*p*-C_6H_4Cl)] (**2**) (left) and K[Ni(GC-OMe)(S-NAc)] (**5**) (right). (Top) Edge spectra displaying the Ni (1s → $4p_z$) transition consistent with square-planar Ni(II). (Middle) EXAFS data. (Bottom) FT k^3 EXAFS data. Experimental data are in black with simulations in red.

Table 2. Ni−K-Edge X-ray Absorption Parameters for Complexes 2 and 5 and [Ni(nmp)(SR)]$^-$ Complexes[38,39] [a]

complex	*n*	shell	R_{as} (Å)	σ_{as}^2 (Å^2)	f' [b]	E_o (eV)	pre-edge peak (eV)	intensity
K[Ni(GC-OMe)(S-*p*-C_6H_4Cl)] (**2**)	1	Ni−N	1.83	0.0024	0.088	8340	8335.8	0.31
	1	Ni−N	1.99	0.0024				
	2	Ni−S	2.16	0.0059				
K[Ni(GC-OMe)(SNAc)] (**5**)	1	Ni−N	1.83	0.0024	0.100	8340	8335.7	0.34
	1	Ni−N	1.99	0.0024				
	2	Ni−S	2.17	0.0052				
K[Ni(nmp)(S-*p*-C_6H_4Cl)]	1	Ni−N	1.85	0.0024	0.075	8340	8337.6	0.42
	1	Ni−N	1.97	0.0024				
	2	Ni−S	2.16	0.0045				
(Et_4N)[Ni(nmp)(S-*o*-babt)]	1	Ni−N	1.86	0.0024	0.061	8340	8336.5	0.42
	1	Ni−N	1.96	0.0024				
	2	Ni−S	2.17	0.0028				
K[Ni(nmp)(S^{t}Bu)]	1	Ni−N	1.85	0.0024	0.076	8340	8336.4	0.35
	1	Ni−N	1.97	0.0024				
	2	Ni−S	2.16	0.0051				

[a] Shell is the chemical unit defined for the multiple scattering calculation. R_{as} is the metal-scatterer distance. σ_{as}^2 is a mean square deviation in R_{as}. [b] f' is a normalized error (chi squared): $f' = (\{\Sigma_i[k^3(\chi_i^{obs} - \chi_i^{calcd})]^2/N\}^{1/2})/([(k^3\chi^{obs})_{max} - (\chi^{calcd})_{min})])$.

monodentate thiolate is lost. Recent mutagenesis studies by Maroney and Brunold on Ni−SOD at Cys2, Cys6, and Cys2/Cys6 (double mutant) have shown that even the absence of one cysteine thiolate promotes a high-spin (S = 1) aquated Ni(II) center at the Ni−SOD active site *with no evidence of the remaining Ni−SCys bond in the single mutants.*[22,24] This finding, in combination with the results reported here, suggests more than redox-modulation/H-storage roles for cysteine in Ni−SOD. We propose that both Cys6 and Cys2 ligands in Ni−SOD are crucial for proper active site assembly and stabilization of the low-spin

dx.doi.org/10.1021/ic2016462 |*Inorg. Chem.* 2011, 50, 10460–10471

square-planar Ni(II) state. This explanation is similar to the advocated H-bond directionality and positioning that Glu17 and Arg47 impart on His1 especially toward formation of the Ni(III)−NHis bond in Ni−SOD_{ox}. Perhaps this hypothesis also explains the various Ni/peptide stoichiometries observed in other Ni−SOD maquettes[31] as well as the chiral inversion seen in the Ni(NCC) tripeptide complex[34] over time. While the hexameric quaternary structure of Ni−SOD likely precludes Cys6 dissociation, cysteinate protonation may be sufficient to trigger weak binding of the His1 imidazole (becoming 5C) to further destabilize the Ni(II) center. The promiscuous nature of these SOD models in buffer underscores the importance of the immediate environment surrounding the active site and points to a role for secondary and tertiary sphere residues in the overall structure and in preserving the integrity and activity of the mononuclear assembly. Various mutagenesis studies on the enzyme have confirmed this notion.[25] Accordingly, the six Ni centers of the Ni−SOD hexamer comprise the vertices of an octahedron with a large interior cavity and are separated by a minimum distance of 23 Å.[18,19] It should be noted that Ni−S complexes are notorious for oligomerization in protic media[51,76] and those containing monodentate thiolate ligands are known to be particularly labile.[55] In fact, to the best of our knowledge, there remains a paucity of literature precedence regarding square-planar Ni complexes featuring monodentate thiolates[62] outside of our work and few pertaining to the characterization of such species in water.

CONCLUSIONS

In summary, the metallopeptide-derived complexes **1**−**5** provide one of the few aqueous studies pertaining to isolable, small-molecule Ni−SOD biomimetics (non-maquette based). The dimeric complex **1** serves as a suitable metallosynthon to generate several unique Ni(II)−N_2S_2 complexes with one variable basal plane coordination site. The electronic absorption spectra of the resulting monomers **2**−**5** in both DMF and pH 7.5 buffer compare well with that obtained for Ni−SOD_{red} and suggest that our $[Ni(GC\text{-}OMe)(SR)]^-$ models have a similar electronic structure to Ni−SOD_{red}. CV measurements in DMF and buffer display irreversible oxidation events within the potential window defined by the SOD half reactions. The CV data suggests that while our mimics are electrochemically capable of promoting SOD chemistry, the Ni(III) state is not accessible, which is crucial for catalysis. Apparently the N_2S_2 planar ligand lacks electrochemical stabilization needed to support a competent SOD mimetic. The failure of our models to provide protection to NBT from superoxide reduction corroborates this notion. This lack of electrochemical reversibility and SOD activity may be attributed to the absence of an axial N-donor or the protective protein shell to stabilize a higher coordinate structure. In fact, flooding these complexes with excess imidazole does not impart any electrochemical reversibility or other spectroscopic changes. The ^{1}H NMR spectra of as-isolated **2**−**5** in D_2O provide broad, ill-resolved signals which may correspond to a variety of species present, perhaps in exchange with one another or with solvent. However, addition of 1 mol-equiv of the appropriate thiolate ligand afforded well-resolved spectra with splitting patterns consistent with a monomeric diamagnetic square-planar species. Dissolution of as-isolated **2**−**5** in CD_3CN afforded neat, readily discernible ^{1}H NMR spectra consistent with discrete species and suggesting further speciation is assisted via interaction with protic media. The NMR data in D_2O coupled with ESI-MS analysis revealed various species of general formula $[Ni_{1-4}(GC\text{-}OMe)_{1-4}(SR)]^-$ and suggest that the active site fragment of Ni−SOD may be a rather dynamic species with a propensity to oligomerize outside of the protein matrix. Thus, the surrounding environment may be crucial to maintaining coordinative integrity. At present, we are undertaking studies pertaining to the role played by the axial imidazole-N donor[77] and exploring ligand modifications with the aim of achieving electrochemical reversibility and ultimately SOD activity.

ASSOCIATED CONTENT

Supporting Information. Full UV−vis spectra of **3** and **5**, full-scale ^{1}H NMR in D_2O and CD_3CN, high-resolution ESI-MS, UV−vis of **2**, **4**, and **5** in buffer with and without added thiolate, and X-ray absorption data for Ni(nmp) complexes. This material is available free of charge via the Internet at http://pubs.acs.org.

AUTHOR INFORMATION

Corresponding Author
*E-mail: tharrop@uga.edu.

ACKNOWLEDGMENT

T.C.H. acknowledges support from the National Science Foundation (NSF CAREER grant CHE-0953102). R.A.S. acknowledges support from the National Institutes of Health (NIH GM042025).

REFERENCES

(1) Beyer, W.; Imlay, J.; Fridovich, I. *Prog. Nucleic Acid Res. Mol. Biol.* **1991**, *40*, 221.
(2) Maritim, A. C.; Sanders, R. A.; Watkins, J. B., III *J. Biochem. Mol. Toxicol.* **2003**, *17*, 24.
(3) Valentine, J. S.; Wertz, D. L.; Lyons, T. J.; Liou, L.-L.; Goto, J. J.; Gralla, E. B. *Curr. Opin. Chem. Biol.* **1998**, *2*, 253.
(4) Kumar, B.; Koul, S.; Khandrika, L.; Meacham, R. B.; Koul, H. K. *Cancer Res.* **2008**, *68*, 1777.
(5) Ishikawa, K.; Takenaga, K.; Akimoto, M.; Koshikawa, N.; Yamaguchi, A.; Imanishi, H.; Nakada, K.; Honma, Y.; Hayashi, J.-I. *Science* **2008**, *320*, 661.
(6) Fortunato, G.; Pastinese, A.; Intrieri, M.; Lofrano, M. M.; Gaeta, G.; Censi, M. B.; Boccalatte, A.; Salvatore, F.; Sacchetti, L. *Clin. Biochem.* **1997**, *30*, 569.
(7) Kocatürk, P. A.; Akbostanci, M. C.; Tan, F.; Kavas, G. O. *Pathophysiology* **2000**, *7*, 63.
(8) Riley, D. P. *Chem. Rev.* **1999**, *99*, 2573.
(9) De Leo, M. E.; Borrello, S.; Passantino, M.; Palazzotti, B.; Mordente, A.; Daniele, A.; Filippini, V.; Galeotti, T.; Masullo, C. *Neurosci. Lett.* **1998**, *250*, 173.
(10) Auchére, F.; Rusnak, F. *J. Biol. Inorg. Chem.* **2002**, *7*, 664.
(11) Tierney, D. L.; Fee, J. A.; Ludwig, M. L.; Penner-Hahn, J. E. *Biochemistry* **1995**, *34*, 1661.
(12) Miller, A.-F. *Curr. Opin. Chem. Biol.* **2004**, *8*, 162.
(13) Borgstahl, G. E. O.; Parge, H. E.; Hickey, M. J.; Beyer, W. F., Jr.; Hallewell, R. A.; Tainer, J. A. *Cell* **1992**, *71*, 107.
(14) Tainer, J. A.; Getzoff, E. D.; Richardson, J. S.; Richardson, D. C. *Nature* **1983**, *306*, 284.
(15) Youn, H.-D.; Youn, H.; Lee, J.-W.; Yim, Y.-I.; Lee, J. K.; Hah, Y. C.; Kang, S.-O. *Arch. Biochem. Biophys.* **1996**, *334*, 341.
(16) Youn, H.-D.; Kim, E.-J.; Roe, J.-H.; Hah, Y. C.; Kang, S.-O. *Biochem. J.* **1996**, *318*, 889.

(17) Palenik, B.; Brahamsha, B.; Larimer, F. W.; Land, M.; Hauser, L.; Chain, P.; Lamerdin, J.; Regala, W.; Allen, E. E.; McCarren, J.; Paulsen, I.; Dufresne, A.; Partensky, F.; Webb, E. A.; Waterbury, J. *Nature* **2003**, *424*, 1037.
(18) Barondeau, D. P.; Kassmann, C. J.; Bruns, C. K.; Tainer, J. A.; Getzoff, E. D. *Biochemistry* **2004**, *43*, 8038.
(19) Wuerges, J.; Lee, J.-W.; Yim, Y.-I.; Yim, H.-S.; Kang, S.-O.; Carugo, K. D. *Proc. Natl. Acad. Sci. U.S.A.* **2004**, *101*, 8569.
(20) Choudhury, S. B.; Lee, J. -W.; Davidson, G.; Yim, Y.-I.; Bose, K.; Sharma, M. L.; Kang, S.-O.; Cabelli, D. E.; Maroney, M. J. *Biochemistry* **1999**, *38*, 3744.
(21) Bryngelson, P. A.; Arobo, S. E.; Pinkham, J. L.; Cabelli, D. E.; Maroney, M. J. *J. Am. Chem. Soc.* **2004**, *126*, 460.
(22) Ryan, K. C.; Johnson, O. E.; Cabelli, D. E.; Brunold, T. C.; Maroney, M. J. *J. Biol. Inorg. Chem.* **2010**, *15*, 795.
(23) Fiedler, A. T.; Bryngelson, P. A.; Maroney, M. J.; Brunold, T. C. *J. Am. Chem. Soc.* **2005**, *127*, 5449.
(24) Johnson, O. E.; Ryan, K. C.; Maroney, M. J.; Brunold, T. C. *J. Biol. Inorg. Chem.* **2010**, *15*, 777.
(25) Herbst, R. W.; Guce, A.; Bryngelson, P. A.; Higgins, K. A.; Ryan, K. C.; Cabelli, D. E.; Garman, S. C.; Maroney, M. J. *Biochemistry* **2009**, *48*, 3354.
(26) Szilagyi, R. K.; Bryngelson, P. A.; Maroney, M. J.; Hedman, B.; Hodgson, K. O.; Solomon, E. I. *J. Am. Chem. Soc.* **2004**, *126*, 3018.
(27) Neupane, K. P.; Shearer, J. *Inorg. Chem.* **2006**, *45*, 10552.
(28) Shearer, J.; Neupane, K. P.; Callan, P. E. *Inorg. Chem.* **2009**, *48*, 10560.
(29) Shearer, J.; Long, L. M. *Inorg. Chem.* **2006**, *45*, 2358.
(30) Neupane, K. P.; Gearty, K.; Francis, A.; Shearer, J. *J. Am. Chem. Soc.* **2007**, *129*, 14605.
(31) Tietze, D.; Breitzke, H.; Imhof, D.; Kothe, E.; Weston, J.; Buntkowsky, G. *Chem.—Eur. J.* **2009**, *15*, 517.
(32) Schmidt, M.; Zahn, S.; Carella, M.; Ohlenschläger, O.; Görlach, M.; Kothe, E.; Weston, J. *ChemBioChem* **2008**, *9*, 2135.
(33) Krause, M. E.; Glass, A. M.; Jackson, T. A.; Laurence, J. S. *Inorg. Chem.* **2010**, *49*, 362.
(34) Krause, M. E.; Glass, A. M.; Jackson, T. A.; Laurence, J. S. *Inorg. Chem.* **2011**, *50*, 2479.
(35) Mathrubootham, V.; Thomas, J.; Staples, R.; McCraken, J.; Shearer, J.; Hegg, E. L. *Inorg. Chem.* **2010**, *49*, 5393.
(36) Shearer, J.; Zhao, N. *Inorg. Chem.* **2006**, *45*, 9637.
(37) Shearer, J.; Dehestani, A.; Abanda, F. *Inorg. Chem.* **2008**, *47*, 2649.
(38) Gale, E. M.; Narendrapurapu, B. S.; Simmonett, A. C.; Schaefer, H. F., III; Harrop, T. C. *Inorg. Chem.* **2010**, *49*, 7080.
(39) Gale, E. M.; Patra, A. K.; Harrop, T. C. *Inorg. Chem.* **2009**, *48*, 5620.
(40) Ma, H.; Chattopadhyay, S.; Petersen, J. L.; Jensen, M. P. *Inorg. Chem.* **2008**, *47*, 7966.
(41) Ma, H.; Wang, G.; Yee, G. T.; Petersen, J. L.; Jensen, M. P. *Inorg. Chim. Acta* **2009**, *362*, 4563.
(42) Pelmenschikov, V.; Siegbahn, P. E. M. *J. Am. Chem. Soc.* **2006**, *128*, 7466.
(43) Mullins, C. S.; Grapperhaus, C. A.; Kozlowski, P. M. *J. Biol. Inorg. Chem.* **2006**, *11*, 617.
(44) Prabhakar, R.; Morokuma, K.; Musaev, D. G. *J. Comput. Chem.* **2006**, *27*, 1438.
(45) Volbeda, A.; Charon, M. H.; Piras, C.; Hatchikian, E. C.; Frey, M.; Fontecilla-Camps, J. C. *Nature* **1995**, *373*, 580.
(46) Ermler, U.; Grabarse, W.; Shima, S.; Goubeaud, M.; Thauer, R. K. *Science* **1997**, *278*, 1457.
(47) Dobbek, H.; Svetlitchnyi, V.; Gremer, L.; Huber, R.; Meyer, O. *Science* **2001**, *293*, 1281.
(48) Doukov, T. I.; Iverson, T. M.; Seravalli, J.; Ragsdale, S. W.; Drennan, C. L. *Science* **2002**, *298*, 567.
(49) Darnault, C.; Volbeda, A.; Kim, E. J.; Legrand, P.; Vernede, X.; Lindahl, P. A.; Fontecilla-Camps, J. C. *Nat. Struct. Biol.* **2003**, *10*, 271.
(50) Krüger, H.-J.; Peng, G.; Holm, R. H. *Inorg. Chem.* **1991**, *30*, 734.
(51) Fox, S.; Wang, Y.; Silver, A.; Millar, M. *J. Am. Chem. Soc.* **1990**, *112*, 3218.
(52) Pavlov, M.; Siegbahn, P. E. M.; Blomberg, M. R. A.; Crabtree, R. H. *J. Am. Chem. Soc.* **1998**, *120*, 548.
(53) Niu, S.; Thomson, L. M.; Hall, M. B. *J. Am. Chem. Soc.* **1999**, *121*, 4000.
(54) Amara, P.; Volbeda, A.; Fontecilla-Camps, J. C.; Field, M. J. *J. Am. Chem. Soc.* **1999**, *121*, 4468.
(55) Rosenfield, S. G.; Armstrong, W. H.; Mascharak, P. K. *Inorg. Chem.* **1986**, *25*, 3014.
(56) O'Reilly, J. E. *Biochim. Biophys. Acta* **1973**, *292*, 509.
(57) Scott, R. A. In *Physical Methods in Bioinorganic Chemistry: Spectroscopy and Magnetism*; Que, L., Jr., Ed.; University Science Books: Sausalito, CA, 2000; p 465.
(58) Ankudinov, A. L.; Ravel, B.; Rehr, J. J.; Conradson, S. D. *Phys. Rev. B* **1998**, *58*, 7565.
(59) Gennari, M.; Orio, M.; Pécaut, J.; Neese, F.; Collomb, M.-N.; Duboc, C. *Inorg. Chem.* **2010**, *49*, 6399.
(60) Jenkins, R. M.; Singleton, M. L.; Almaraz, E.; Reibenspies, J. H.; Darensbourg, M. Y. *Inorg. Chem.* **2009**, *48*, 7280.
(61) Jenkins, R. M.; Singleton, M. L.; Leamer, L. A.; Reibenspies, J. H.; Darensbourg, M. Y. *Inorg. Chem.* **2010**, *49*, 5503.
(62) Huang, D.; Deng, L.; Sun, J.; Holm, R. H. *Inorg. Chem.* **2009**, *48*, 6159.
(63) Baidya, N.; Olmstead, M. M.; Mascharak, P. K. *Inorg. Chem.* **1991**, *30*, 3967.
(64) Silverstein, R. M.; Webster, F. X.; Kiemle, D. J. *Spectrometric Identification of Organic Compounds*; Wiley: Hoboken, NJ, 2005.
(65) Mills, D. K.; Reibenspies, J. H.; Darensbourg, M. Y. *Inorg. Chem.* **1990**, *29*, 4364.
(66) Smee, J. J.; Miller, M. L.; Grapperhaus, C. A.; Reibenspies, J. H.; Darensbourg, M. Y. *Inorg. Chem.* **2001**, *40*, 3601.
(67) Farmer, P. J.; Reibenspies, J. H.; Lindahl, P. A.; Darensbourg, M. Y. *J. Am. Chem. Soc.* **1993**, *115*, 4665.
(68) Grapperhaus, C. A.; Maguire, M. J.; Tuntulani, T.; Darensbourg, M. Y. *Inorg. Chem.* **1997**, *36*, 1860.
(69) Colpas, G. J.; Kumar, M.; Day, R. O.; Maroney, M. J. *Inorg. Chem.* **1990**, *29*, 4779.
(70) Hanss, J.; Krüger, H.-J. *Angew. Chem., Int. Ed.* **1998**, *37*, 360.
(71) Maroney, M. J.; Choudhury, S. B.; Bryngelson, P. A.; Mirza, S. A.; Sherrod, M. J. *Inorg. Chem.* **1996**, *35*, 1073.
(72) Sawyer, D. T.; Valentine, J. S. *Acc. Chem. Res.* **1981**, *14*, 393.
(73) Tabbì, G.; Driessen, W. L.; Reedijk, J.; Bonomo, R. P.; Veldman, N.; Spek, A. L. *Inorg. Chem.* **1997**, *36*, 1168.
(74) Gu, Z.; Dong, J.; Allan, C. B.; Choudhury, S. B.; Franco, R.; Moura, J. J. G.; Moura, I.; LeGall, J.; Przybyla, A. E.; Roseboom, W.; Albracht, S. P. J.; Axley, M. J.; Scott, R. A.; Maroney, M. J. *J. Am. Chem. Soc.* **1996**, *118*, 11155.
(75) Colpas, G. J.; Maroney, M. J.; Bagyinka, C.; Kumar, M.; Willis, W. S.; Suib, S. L.; Baidya, N.; Mascharak, P. K. *Inorg. Chem.* **1991**, *30*, 920.
(76) Tremel, W.; Kriege, M.; Krebs, B.; Henkel, G. *Inorg. Chem.* **1988**, *27*, 3886.
(77) Gale, E. M.; Simmonett, A. C.; Telser, J.; Schaefer, H. F., III; Harrop, T. C. *Inorg. Chem.* **2011**, *50*, in press (http://dx.doi.org/10.1021/ic201822f).